

The following document contains a manuscript that was submitted to *Paleoceanography and Paleoclimatology* on 2020-07-27 and is currently subject to an ongoing peer-review process.

Modeling the impact of bioturbation and species abundance upon discrete-depth individual foraminifera analysis used in ENSO-type climate reconstructions.

B.C. Lougheed¹ and B. Metcalfe²

1. Department of Earth Sciences, Uppsala University, Sweden.

2. Department of Earth Sciences, Vrije Universiteit Amsterdam, the Netherlands.

Corresponding author: B.C. Lougheed (bryan.lougheed@geo.uu.se)

Abstract

We use a single foraminifera enabled, holistic hydroclimate-to-sediment transient modelling approach to fundamentally evaluate the efficacy of discrete-depth individual foraminifera analysis (IFA) for reconstructing past sea surface temperature (SST) distribution, a method that has been used for reconstructing El Niño Southern Oscillation (ENSO). The computer model environment allows us to control for variables such as sea surface temperature (SST), foraminifera species abundance response to SST, as well as depositional processes such as sediment accumulation rate (SAR) and bioturbation depth (BD), and subsequent laboratory processes such as sample size and machine error. Examining a number of best-case scenarios, we find that IFA-derived reconstructions of past SST distribution are sensitive to all of the aforementioned variables. Running 100 ensembles for each scenario, we find that the influence of bioturbation upon IFA-derived SST reconstructions, combined with typical samples sizes employed in the field, produces noisy SST reconstructions with poor correlation to the true SST distribution in the water. This noise is especially apparent for values near the edge of the SST distribution, which also happens to be the distribution region of particular interest for ENSO. The noise is further increased in the case of machine error and decreasing SAR. We also find poor agreement between ensembles, underscoring the need for replication studies in the field to confirm findings at particular sites and time periods. Furthermore, we show that a species' abundance response to SST could bias IFA-derived SST reconstructions, which can have consequences when comparing IFA-derived SST from markedly different mean climate states.

Plain language summary

30 Measurements on individual sea-dwelling shelled organisms called foraminifera retrieved from deep-sea
sediment cores have been used to reconstruct past water temperature variation and, in turn, past El Niño.
To evaluate this method, we use a computer model to simulate millions of single foraminifera and how
they become mixed in the sediment after being deposited upon the sea floor. This approach allows us to
subsequently compare the water temperature reconstructed from the single foraminifera in the sediment
35 core to the true water temperature in the water during the past. In short, our computer simulation helps to
define the total uncertainty associated with El Niño reconstructions based on such methods.

1.0 Introduction

1.1 Background

40 El Niño Southern Oscillation (ENSO) is an important feature of the Earth's interannual climate dynamics,
and the magnitude of ENSO events has important consequences for human populations of the tropical
Pacific regions and further afield (Lyon & Barnston, 2005). Future climate change may impact the
magnitude and/or frequency of climate events. ENSO manifests itself as a reversal of the Pacific trade
winds and associated extreme shifts in tropical Pacific sea surface temperature (SST) patterns, with
observational era ENSO events having occurred every two to seven years, and being between nine and 12
months in duration. Knowledge of ancient monthly SST variation and its relationship with past global
45 climate parameters is therefore crucial in advancing our understanding of palaeo-ENSO dynamics and,
thus, better informing future regional climate predictions (Rosenthal & Broccoli, 2004). To this end,
forensic palaeoceanographic analysis of pan-Pacific deep-sea sediment can potentially offer a pan-Pacific
archive of past frequency and magnitude of SST extremes and their relationship to past global climate
conditions, potentially providing valuable insight into past ENSO.

50 The most-studied palaeoclimate signal carrier vessel within deep-sea sediment cores is the carbonate
shells of planktonic foraminifera (microscopic, single-celled organisms), which can record the conditions
of the ambient water that the foraminifera lived in. These organisms have a lifespan of ~1 month, after
which their shells are deposited on the sea-floor. Their short lifespan means that foraminifera populations
retrieved from deep-sea sediment archives can, in principle, reflect past monthly SST dynamics, which is
55 key for reconstructing ENSO events. However, the technical limits associated with isotope ratio mass
spectrometry (IRMS) analysis of foraminifera has traditionally required that many tens of single
foraminifera shells to produce a viable measurement, thus averaging out any monthly SST signal.
Advances in IRMS have allowed for the analysis of single foraminifera shells of sizes representative of
planktonic populations (Oba & Uomonoto, 1989; Spero & Williams, 1990), which has encouraged
60 researchers to carry out individual foraminifera analysis (IFA) to reconstruct SST variability associated

with ENSO (Koutavas et al., 2006; Leduc et al., 2009). This method can, in principle, allow for the extraction of a range of monthly SST values from a given interval of a deep-sea sediment archive (i.e. 1 cm discrete depths from a given sediment core). Using the IFA method, a number of foraminifera are sub-sampled from a discrete-depth's foraminifera population, after which some form of proxy method is applied to each foraminifera's carbonate shell to infer individual SST values.

The IFA method depends upon a major assumption, namely that the distribution of the sub-sampled foraminifera SST values are a faithful representation of the true distribution of monthly SST values for a given time interval (i.e. a decadal/centennial/millennial period). The ability of discrete-depth IFA to accurately reproduce a time period's true SST distribution can be clouded by a number of environmental, biological and logistical issues, which occur in the water domain (pre-deposition), sediment archive domain (post-deposition) and laboratory domain (post-retrieval). Regarding issues in the water domain, it is possible that a foraminifera species may not exist continually at a single surface water location, thus giving a non-continuous record of SST, which can have consequences for ENSO reconstructions (Metcalf et al., 2020). Secondly, a species' foraminiferal abundance through time is not constant and can be influenced by SST itself, which may bias IFA-derived SST distribution reconstructions, which is especially relevant in the case of ENSO, which itself influences SST. Similarly, long-term absolute shifts in the overall range of SST (e.g. from a glacial to an interglacial world) may cause the water's SST range to shift from one that partially overlaps with a species' preferred temperature range to one that fully overlaps with a species' preferred temperature range. In practical terms, this could lead to an IFA-derived artefactual shift from a relatively narrow SST range to a relatively wider SST range, with potential for incorrect interpretation regarding glacial-interglacial ENSO dynamics.

Issues associated with the sediment archive domain can further cloud IFA-derived SST distributions. Specifically, systematic bioturbation of deep-sea sediment archives means that individual foraminifera with vastly different ages are mixed into single discrete-depth sediment intervals, which is a particular challenge in the current state-of-the-art in IFA, which still relies on the 'average age' of a particular sediment interval (i.e. it is not yet feasible to systematically date single planktonic foraminifera). This practical limitation in turn places an interpretive constraint upon IFA; when foraminifera from vastly different long-term climate states (i.e. multi-millennial) are mixed into the same sediment interval, IFA-derived SST variability reconstructed from that sediment interval cannot be exclusively assigned to decadal or centennial changes in ENSO dynamics. For these reasons, it is important to understand the age distribution of the foraminifera contained within a discrete-depth sediment interval. For example, it is often assumed that a sediment archive with a sediment accumulation rate (SAR) of e.g. 5 cm ka⁻¹ will have a temporal resolution of $1000/5 = 200$ yr cm⁻¹, an assumption that is deceptively supported the

95 observation that the mean age of such a sediment archive would increase by ~ 200 yr every cm. However,
downcore discrete-depth change in mean age is not the same concept as variance of the age contained
within a single discrete-depth of sediment. The distribution of the age contained within a single
centimetre of sediment core is governed not only by the SAR, but also by the bioturbation depth (BD), the
uppermost depth of the sediment within which bottom-dwelling organisms actively mix the sediment.
Following established understanding of bioturbation processes (Berger & Heath, 1968; Pisias, 1983;
100 Schiffelbein, 1984), the 1σ age value for a single cm of sediment core can be approximated, in the
example of a 5 cm ka^{-1} sediment core with a representative BD of 10 cm (Boudreau, 1998; Trauth et al.,
1997), as $10/5 \times 1000 = 2000$ yr. In idealised conditions, the corresponding shape of the age distribution
for a discrete-depth interval of sediment core will be characterised by an exponential distribution with
long tail towards older ages. The average age of the sediment at the top of the sediment archive will also
105 be similar to the 1σ age value, as exhibited in ^{14}C dates of deep-sea core tops which support a BD of
between 5 and 10 cm (Henderiks et al., 2002; Trauth et al., 1997), including for the Pacific (Peng et al.,
1979; White et al., 2018). It is additionally important to consider the shape of this distribution when
comparing IFA-derived SST from an interval of sediment core (subsamped from a population with a
exponential age distribution with a long tail towards older ages) to observational or model SST from
110 specific periods of climate history (i.e. a uniform interval of time).

1.2 Experimental Design

Here, we use a computer modelling approach, which allows all simulation parameters to be known and
strictly controlled, thereby allowing us to create an idealised experimental design with minimised degrees
of freedom. Such an experimental design takes advantage of computer modelling as an investigative tool
115 with which to increase our conceptual understanding of processes (Emanuel, 2020). This approach offers
advantages over field-based testing of IFA, the latter of which is affected by multiple dynamic
parameters, thus leading to increased degrees of freedom and limiting the ability to make interpretative
conclusions. Our comprehensive modelling approach incorporates controlled parameterisations of
climate, sediment and laboratory processes. Such a strictly-controlled computer model environment
120 allows us to directly compare a known input SST signal to a reconstructed SST derived from the
corresponding simulated sediment-based IFA incorporating known understanding of sediment concepts.
In this way, we can objectively quantify how well field-based discrete-depth IFA would function in a
number of best-case scenarios, allowing its interpretive capacity for the reconstruction of ENSO-type
climate variability to be evaluated at the most fundamental level.

125 2.0 Method

2.1 Approach synopsis and model setup

We carry out a holistic hydroclimate-to-sediment transient modelling approach to test the suitability of discrete-depth IFA for the reconstruction of ENSO-type climate variability. Crucially, our approach includes a quantified representation of both sediment dynamics (in particular bioturbation) and species abundance, thus building upon previous models and simulation estimations of IFA accuracy where such information was not yet included (Fraass & Lowery, 2017; Leduc et al., 2009; Thirumalai et al., 2013). Our modelling approach is carried out using an offline coupling of two transient models: a single-foraminifera sediment accumulation simulator (SEAMUS; (Lougheed, 2020)) run at a monthly timestep resolution, forced with monthly SST from the TRACE-21ka climate model (He, 2011). We investigate a number of best-case scenarios, concentrating on the time period spanning from 20 ka (BP 1950) up to and including 1989 CE, assuming a hypothetical sediment core at a location ideal for studying ENSO (Fig. 1), i.e. at the centre of the Niño 3.4 ENSO region that is used to calculate the Oceanic Niño Index (ONI).

In this study, simulated single foraminifera are incorporated into synthetic sediment archives, the latter of which employ best-case sedimentation conditions whereby representative values for SAR and BD are both kept temporally constant. We assume a best-case scenario where foraminifera perfectly record monthly SST (in this case the TRACE-21ka SST), and we also assume the existence of an ideal proxy method that allows for perfect retrieval of SST data from the single foraminifera. In reality, foraminifera may not continuously record the water temperature at the surface or indeed at the same water depth in general, which further complicates IFA ENSO in practice, however, here we seek to test best case conditions. After carrying out the sediment archive and bioturbation simulation, synthetic single foraminifera are randomly picked from each discrete-depth cm interval of simulated core, thereby resulting in virtual IFA. The output of the best-case virtual IFA retrieved from the sediment depth domain can subsequently be directly compared to the inputted SST in the time domain (i.e. TRACE-21ka SST), allowing us to evaluate the current state-of-the-art in IFA at the most fundamental level.

We sum up the sediment model component (SEAMUS) in Section 2.1, and the climate component (TRACE-21ka) in Section 2.2. An overview of our various best-case scenario simulations, as well as their associated run parameters, can be found in Section 2.3.

2.1 Sediment model component

We model the sedimentation history of single foraminifera using the the SEAMUS sediment accumulation model (Lougheed, 2020). This stochastic model uses the same established understanding of bioturbation (Bard, 2001; Berger & Heath, 1968; Pisias, 1983) that is also incorporated into previous

sediment accumulation models (Dolman & Laepple, 2018; Trauth, 1998, 2013), but differs in model execution in that it is explicitly designed for the purpose of modelling single foraminifera, thus making it a suitable sediment model for use in this IFA evaluation study. Furthermore, the stochastic nature of the model is ideal for simulating bioturbation of single foraminifera, which is in itself a stochastic process. Our period of interest spans 20 ka BP to 1990 CE, so we have run the SEAMUS model from 30 ka BP to 1990 CE to provide sufficient model spin-up for our period of interest. The model is run using a monthly timestep resolution, whereby single synthetic foraminifera are generated at each time-step and added to the top of the sediment archive after which the BD of the sediment archive is uniformly mixed. All simulations are run with an appropriate BD of 10 cm, following previous studies (Boudreau, 1998; Trauth et al., 1997). Some of our model run scenarios assume a temporally constant foraminiferal abundance, in such cases we assign a constant per timestep foraminiferal abundance that results in 10^4 foraminifera per cm of sediment (i.e. the prescribed per timestep abundance is higher in the case of higher SAR and vice-versa). In the case of model runs with temporally dynamic foraminiferal abundance, 100 foraminifera per timestep (i.e. month) are simulated, allowing temporal (i.e. monthly) changes in abundance to be modelled with sufficient statistical power (i.e. if relative abundance of a the species drops from 0.56 to 0.55 then it will result in one less foraminifera of the species being simulated for a timestep). All of our model run scenarios are carried out using 100 ensemble runs in SEAMUS, thus capturing the stochastic nature of bioturbation (i.e. the fact that no two sediment archives formed under the same conditions will be exactly alike). Subsequently, four separate ‘picking’ scenarios are carried out on each of the 100 ensembles, whereby 50, 100, 500 or 10^4 synthetic foraminifera are randomly picked from each discrete 1 cm depth slice of the synthetic core, whereby the picker is assumed to have perfectly identified the species in all cases, thus avoiding challenges associated with species mis-identification (Pracht et al., 2019). Finally, in some scenarios we add Gaussian noise of $\pm 1^\circ\text{C}$ to the SST of all simulated foraminifera, to mimic proxy uncertainty (approximately equivalent to a $\delta^{18}\text{O}$ measurement error of 0.1‰). Ensemble runs were performed using a computer cluster provided by the Swedish National Infrastructure for Computing (SNIC) at the Uppsala Multidisciplinary Centre for Advanced Computational Science (UPPMAX).

2.2 Climate model component

Monthly SST forcing for the SEAMUS model is sourced from the TRACE-21ka transient climate simulation (He, 2011), specifically using the surface temperature data for the TRACE-21ka grid cell centred on the coordinates 1.86° N and 146.25° W . This grid cell, at the centre of the Niño 3.4 ENSO region used for calculating the ONI-index, is ideal for our synthetic core simulation as it is characterised by high inter-annual surface temperature variation typical of ENSO (Fig. 1a). Furthermore, the grid cell

190

also captures the glacial-interglacial SST transition (Fig. 1b), as well as typical TRACE-21ka transient changes in ENSO-type SST dynamics, as shown by the 1.5-7 yr filtered 100 and 1000 year moving 1σ of SST (Fig. 1c). This filtering approach has previously been used to identify ENSO-type dynamics in TRACE-21ka for the Niño 3.4 region (Liu et al., 2014).

195

The TRACE-21ka dataset is the result of a fully-coupled Community Climate System Model (CCSM3) simulation with T31_gx3 grid resolution that uses transient forcing changes in both greenhouses gases, orbital driven insolation variations, ice sheet evolution (ICE-5G) and associated meltwater fluxes for a non-accelerated atmosphere-ocean-sea ice-land surface coupling. The TRACE-21ka dataset begins at 22 ka, whereas our SEAMUS run starts at 30 ka. The reason for this difference is that our period of interest for this study covers the period spanning the past 20 ka, and we provide an extra 10 ka of spin-up time for the SEAMUS model, which is important in cases of very low SAR (e.g. $\leq 5 \text{ cm ka}^{-1}$). In order to provide SST data for synthetic foraminifera generated between 30 ka and 22 ka, the oldest 1500 years contained within the TRACE-21ka dataset are repeated from 22 ka to 30 ka. Such an approach obviously does not represent an accurate picture of the climate between 30 ka and 22 ka, but it has no practical consequences for the particular purpose of our study, which is to compare a given climate input signal in the time domain to the subsequent signal recorded by single foraminifera in the sediment depth domain. Furthermore, our period of study interest spans the past 20 ka.

200

205

2.3 Model run settings

210

We carry out a number of best-case scenarios, with each scenario being subject to 100 ensemble runs to capture the full stochastic range resulting from the sedimentation, bioturbation and picking process. We run SAR scenarios for 5, 10 and 40 cm ka^{-1} . In this study, we concentrate on best-case scenarios, so the figures in the main text are for the 40 cm ka^{-1} scenarios only. The corresponding figures for the 5 cm ka^{-1} and 10 cm ka^{-1} scenarios, which may be more realistic for much of the Pacific, can be found in the supplement. Each of the three SAR scenarios is first subjected to 100 ensemble runs with constant foraminifera abundance and a perfect SST proxy, a second set of 100 ensemble runs is then carried out with constant abundance and added $\pm 1^\circ\text{C}$ Gaussian noise on the SST proxy, a third set of 100 ensemble runs is carried out with dynamic abundance and a perfect SST proxy, and a final set of 100 ensemble runs is carried out with dynamic abundance and $\pm 1^\circ\text{C}$ Gaussian noise on the SST proxy. All of the aforementioned 1200 ensembles are each subjected to randomised picking for 50, 100, 500 and 10^4 foraminifera per cm of sediment core depth.

215

220

As described in the previous paragraph, some of our scenarios incorporate dynamic foraminiferal abundance in order to investigate the effect of changes in species abundance upon IFA-derived

reconstructions. In these scenarios, we use a hypothetical transfer function (Fig. 2a) to assign a per timestep abundance to our simulated foraminifera species, whereby the abundance is calculated as a function of the corresponding TRACE-21ka SST for the timestep. This approach allows us to quantify how a known species abundance response to SST could systematically bias an IFA-derived SST distribution. Consider, for example, a theoretical time interval whereby the true monthly SST data are normally distributed, as in the theoretical example in Fig. 2b. In such a case, an IFA-derived SST distribution using a species characterised by our SST transfer function would be biased towards warmer temperatures and, furthermore, the shape of the IFA-derived SST distribution would be skewed, as shown in the abundance-modified profile in Fig. 2b.

3.0 Results & Discussion

3.1 Downcore, discrete-depth IFA standard deviation

Numerous studies have concentrated on subsampling numerous individual foraminifera from the same discrete-depth interval of a sediment core, from which the 1σ value of the SST (or a proxy equivalent thereof) of those foraminifera is calculated to infer ENSO activity for a particular time period, whereby a greater 1σ value is assumed to indicate increased ENSO activity, and vice versa (Koutavas et al., 2006; Koutavas & Joanides, 2012; Rustic et al., 2015). To evaluate such an approach, we compare the 1.5-7 yr filtered 1000 year moving 1σ of SST in the time domain (Fig. 1c) to ensembles of SEAMUS runs carried out under various sediment and picking conditions within a best-case 40 cm ka^{-1} scenario (Fig. 3 and Fig. 4). The equivalent figures for the 5 cm ka^{-1} and 10 cm ka^{-1} scenarios, which may more be representative best-case values for the open ocean areas of the Pacific (Metcalf et al., 2020), can be found in the supplement.

We find that the discrete-depth, downcore 1σ value reconstructed using IFA analysis for the simulated 40 cm/ ka scenarios varies greatly between all of the 100 ensemble runs in the case of IFA sample sizes typically used in the field, i.e. between 50 foraminifera (Fig. 3a-b; Fig. 4a-b) and 100 foraminifera (Fig. 3c-d; Fig. 4c-d) individual foraminifera being picked per cm. This poor reproducibility between ensemble runs is a result of noise generated by small sample sizes in combination with systematic bioturbation. The practical consequence of this poor reproducibility is that, in the case of typical sample sizes used in the field (50-100 foraminifera), none or very few of the 100 ensemble runs result a significant correlation (here, $r^2 \geq 0.6$ and $p \leq 0.05$) between the IFA-derived downcore 1σ SST signal and the 1.5-7 yr filtered TRACE-21ka 1000 year moving 1σ (Table 2), for the period 18 ka to 12 ka, a period of dynamic ENSO-type variation in the TRACE-21ka SST. Furthermore, the wide 95.4% band of ensemble downcore 1σ SST values demonstrates a practical challenge for studies that compare ENSO conditions from two

255 distinct time periods by comparing, e.g., a late glacial sediment slice's 1σ SST value to a late Holocene
sediment slice's 1σ SST value. In such cases, our model results suggest that, for the aforementioned
typical sample sizes deployed in the field (50-100 foraminifera), random chance may lead to any number
of possible apparent outcomes regarding the relative apparent ENSO states of the late glacial and the late
Holocene.

260 We do find, however, that greatly increased sample size, higher SAR and reduced measurement error can
all significantly improve the probability of a given ensemble's IFA-derived downcore 1σ SST exhibiting
significant correlation with the TRACE-21ka SST ENSO-type variation (Table 2). We must stress,
however, that our best-case scenarios involve constant SAR and BD, whereas real world conditions in the
field are inherently dynamic and would, therefore, be even more challenging, even in the case of larger
sample sizes. Additionally, we note that the improved correlation in the case of larger samples size does
265 not correspond to a good reproduction of the *absolute* values of the ENSO-type variation as indicated by
the TRACE-21ka SST ENSO-type variation. We note that even in the case of an extreme best-case
scenario where it is possible to find, pick and analyse 10^4 foraminifera per cm, the absolute values of the
ENSO-type variation derived from IFA are systematically greater than that of the TRACE-21ka SST
ENSO-type variation (Fig. 3g and Fig. 4g), despite good correlation (Table X). This offset in absolute
270 values can be due to the fact that the 1.5-7 yr filtered, 1000 year smoothed TRACE-21ka standard
deviation is reflecting a different integration of the time than the 1σ data retrieved from discrete-depth
IFA. The former is based on a smooth of uniform time, whereas the latter represents a population of
foraminifera with a long-tailed age distribution. The absolute offset between the two signals is further
increased in the case of machine error on the IFA SST analysis (Fig. 3h and Fig. 4h), thus highlighting the
275 importance of accurately quantifying uncertainties in the analytical process.

3.2 Discrete-depth IFA distribution analysis

280 Many IFA studies have gone beyond studying a discrete depth's 1σ SST value and have branched into
more forensic studies of a discrete depth's IFA-derived SST distribution. These studies have focussed on
analysing the shape of said distribution using various statistical tools, including histograms to infer
distribution skewness analysis of histograms (Khider et al., 2011; Leduc et al., 2009), as well as quantile-
quantile (Q-Q) plots (Ford et al., 2015; Rongstad et al., 2020; Thirumalai et al., 2019; White et al., 2018;
White & Ravelo, 2020). Such analysis can reveal apparent shifts in the shape of the downcore, IFA-
derived SST distribution, which the aforementioned studies have attributed to changes in ENSO-type
climate variability.

285 Here, we compare the monthly TRACE-21ka SST data for the 18 ka to 17 ka period to our 100 ensembles
of simulated IFA SST for our 40 cm ka⁻¹ scenario, taking in each ensemble the 1 cm discrete-depth with a
median age closest to 17.5 ka. We detail 100 ensembles with no analytical error and constant abundance
(Fig. 5), 100 ensembles with ±1° C analytical error and constant abundance (Fig. 6), 100 ensembles with
290 ±1° C analytical error and dynamic abundance (Fig. 7), and 100 ensembles with ±1° C analytical error
and dynamic abundance (Fig. 8). In all cases in our 40 cm ka⁻¹ scenario, we find that sample sizes
typically associated with IFA in the field (50-100 foraminifera) produce high levels of noise, leading to
low reproducibility from one ensemble to the next (panels a and d in Figs. 5-8), with even lower
reproducibility in the case of the 5 and 10 cm ka⁻¹ scenarios (see supplemental figures). In practical terms,
these results suggest that if one were to, at the same coring location, retrieve multiple sediment cores and
295 carry out discrete-depth IFA, it is likely that markedly different outcomes would be produced each time,
each with poor correspondence to the true SST distribution. Furthermore, as the level of noise increases
with lower SAR, one has to be additionally careful when comparing IFA results from sites with markedly
different SAR (Thirumalai et al., 2019).

We also find that the IFA method has a tendency for noisy over- or undersampling of the tails of the true
300 SST distribution in the case of typical sample sizes (50-100 specimens) used in the field (panels b and e
in Fig. 5-8). This effect can be attributed to the fact that there is a low occurrence of individual
foraminifera within the population that record more extreme temperatures, and small sample sizes are
likely to either miss such foraminifera altogether (i.e., -100% oversampling), or, in the case of a single
such foraminifera being picked within the sample, significantly over-represent extreme SST within the
305 sample (in some cases >500% oversampling). This effect has practical consequences for interpretations
made within IFA studies, seeing as the tails of the SST distribution also happen to be the region of
interest when reconstructing the presence of extreme ENSO events (Koutavas et al., 2006; Rustic et al.,
2015). This noisy under- or oversampling of the distribution tails by IFA also translates directly to sample
Q-Q plots (panels c and f in Fig. 5-8), which are commonly used in IFA studies to investigate the
310 population distribution (Ford et al., 2015; Rongstad et al., 2020). This level of noise in the tails increases
substantially in the case of increased analytical error, i.e. when one compares panels a-f in Fig 5 (without
simulated analysis error) and Fig. 6 (with ±1°C simulated analysis error). We furthermore find that even
larger sample sizes involving 500 foraminifera are also prone to noisy under- or oversampling in the tails,
especially in the case of analytical error (panels g, h, and i in Fig. 6). We also note that the tendency for
315 under- and oversampling in the tails is greatly increased in the case of lower SAR that is more
representative of real-world conditions (see supplemental figures for 5 cm ka⁻¹ and 10 cm ka⁻¹ SAR
scenarios). Even in the case of sample sizes of 10⁴ foraminifera in our 40 cm ka⁻¹ scenario (panels j, k and
l in Figs. 5 and 6) we also find sub-optimal agreement with the TRACE-21ka SST distribution in the tails.

320 This disagreement is not due to noise, but due to the fact that we emulate the current state of the art, whereby researchers compare SST from a uniform interval of time (in our case 18 ka to 17 ka) to a sample of foraminifera retrieved from a discrete-depth with a foraminifera population characterised not by a uniform distribution, but an exponential distribution with a long tail towards older ages.

325 Finally, we investigate the influence of temperature-induced species abundance changes upon IFA-derived SST distributions. Our 40 cm ka⁻¹ simulations that have been run using the temperature abundance transfer function in Fig. 2a are shown in Fig. 7 (without analytical noise) and Fig. 8 (with analytical noise). We find that in all cases, the IFA-derived SST distribution is biased towards too warm values when compared to the TRACE-21ka SST distribution (panels a, d, g and j in Fig. 7 and Fig. 8). This bias can also be visualised as an oversampling of warmer values (panels b, e, h, k in Fig. 7 and Fig. 8), or bias in a Q-Q plot (panels c, f, i, l in Fig. 7 and Fig. 8). We demonstrate that a species' abundance response to temperature can inherently bias IFA-derived reconstructions of SST distribution, which could have practical consequences for studies in the field. For example, the results in studies that compare IFA-derived SST distributions from significantly differing mean climate states (White et al., 2018; White & Ravelo, 2020), may be (partially) attributable to a species' temperature abundance response to the dominating SST profile associated with the differing climate states. Our results demonstrate the importance of incorporating understanding of past temporal changes of species abundance and its relationship to past SST to better constrain such studies.

330 4.0 Conclusion

335 Our best-case modelling study reveals a number of challenges which inhibit the efficacy of discrete-depth IFA in producing reconstructions of past SST distribution, the latter of which is paramount in reconstructing past ENSO-type climate dynamics. Firstly, we find that bioturbation of sediment archives, combined with typical sample sizes employed in IFA-based studies, can lead to noisy IFA-derived SST distribution reconstructions. This noise leads to poor reproducibility with a potential for artefactual results. We propose that this problem can be addressed by quantifying the total error on IFA-reconstructions using two main approaches: (1) Ensemble-based forward model studies, as detailed in this study using best-case scenarios, can be run using the dynamic sediment and species abundance parameters present at a particular archive in the field. This approach will help estimate the total stochastic error associated with the IFA-derived reconstruction. Care must be taken to include uncertainties regarding time-domain estimations of SAR, BD, species abundance, and analytical uncertainty. (2) Replication studies in the field (essentially a real-world ensemble approach) can help to further understand of the the stochastic noise involved with IFA reconstructions.

355 We furthermore have shown in our best-case study that a species' abundance response to SST can inherently bias IFA-derived reconstructions of past SST variance. We propose that the coupling of a single foraminifera sediment model approach to foraminiferal ecological models (Lombard et al., 2011; Metcalfe et al., 2020; Roche et al., 2018) could further help to constrain the total uncertainty associated with IFA-derived SST reconstructions.

360 We have also demonstrated that SST from uniform periods of time (as humans are accustomed to using) cannot directly be compared to IFA-derived SST which is retrieved from a population with an age distribution characterised by an exponential distribution with a long tail towards older ages. Subsequently, we propose that researchers adjust observational or model SST data to integrate an exponential representation of time when comparing to IFA-derived SST.

365 Finally, we note that although our study concentrates on the IFA method, our results are also useful for researchers who measure pooled samples of foraminifera (i.e. measurement upon multi-specimen samples) to reproduce a general SST history in the Pacific. Our ensemble results help shine light upon the intra-sample variability that could be expected within such samples, as well as possible noise artefacts present in the mean value.

Author contributions

BCL and BM conceived the study. BCL executed the model runs and wrote the manuscript, with input from BM.

Acknowledgements

370 BCL acknowledges Swedish Research Council (Vetenskapsrådet – VR) Starting Grant number 2018-04992. The Swedish National Infrastructure for Computing (SNIC) at the Uppsala Multidisciplinary Centre for Advanced Computational Science (UPPMAX) provided computing resources for parallel ensemble runs. Jesper Sjolte and Feng He are thanked for help in locating the correct TRACE-21ka model run file.

Data availability

375 No new data have been generated in this study.

References

- Bard, E. (2001). Paleooceanographic implications of the difference in deep-sea sediment mixing between large and fine particles. *Paleoceanography*, *16*(3), 235–239.
- Berger, W. H., & Heath, G. R. (1968). Vertical mixing in pelagic sediments. *Journal of Marine Research*, *26*, 134–143.
- Boudreau, B. P. (1998). Mean mixed depth of sediments: The wherefore and the why. *Limnology and Oceanography*, *43*(3), 524–526. <https://doi.org/10.4319/lo.1998.43.3.0524>
- Dolman, A. M., & Laepple, T. (2018). Sedproxy: a forward model for sediment archived climate proxies. *Climate of the Past Discussions*, 1–31. <https://doi.org/10.5194/cp-2018-13>
- Emanuel, K. (2020). The Relevance of Theory for Contemporary Research in Atmospheres, Oceans, and Climate. *AGU Advances*, *1*(2), e2019AV000129. <https://doi.org/10.1029/2019AV000129>
- Ford, H. L., Ravelo, A. C., & Polissar, P. J. (2015). Reduced El Nino-Southern Oscillation during the Last Glacial Maximum. *Science*, *347*(6219), 255–258. <https://doi.org/10.1126/science.1258437>
- Fraass, A. J., & Lowery, C. M. (2017). Defining uncertainty and error in planktic foraminiferal oxygen isotope measurements: Uncertainty in Foram Oxygen Isotopes. *Paleoceanography*, *32*(2), 104–122. <https://doi.org/10.1002/2016PA003035>
- Ganssen, G. M., Peeters, F. J. C., Metcalfe, B., Anand, P., Jung, S. J. A., Kroon, D., & Brummer, G.-J. A. (2011). Quantifying sea surface temperature ranges of the Arabian Sea for the past 20 000 years. *Climate of the Past*, *7*(4), 1337–1349. <https://doi.org/10.5194/cp-7-1337-2011>
- He, F. (2011). *Simulating transient climate evolution of the last deglaciation with CCSM 3* (Ph.D. thesis). University of Wisconsin - Madison, Madison, WI, USA.
- Henderiks, J., Freudenthal, T., Meggers, H., Nave, S., Abrantes, F., Bollmann, J., & Thierstein, H. R. (2002). Glacial–interglacial variability of particle accumulation in the Canary Basin: a time-slice approach. *Deep Sea Research Part II: Topical Studies in Oceanography*, *49*(17), 3675–3705. [https://doi.org/10.1016/S0967-0645\(02\)00102-9](https://doi.org/10.1016/S0967-0645(02)00102-9)

- Khider, D., Stott, L. D., Emile-Geay, J., Thunell, R., & Hammond, D. E. (2011). Assessing El Niño Southern Oscillation variability during the past millennium. *Paleoceanography*, *26*(3).
<https://doi.org/10.1029/2011PA002139>
- Koutavas, A., & Joanides, S. (2012). El Niño–Southern Oscillation extrema in the Holocene and Last Glacial Maximum. *Paleoceanography*, *27*(4). <https://doi.org/10.1029/2012PA002378>
- Koutavas, A., deMenocal, P. B., Olive, G. C., & Lynch-Stieglitz, J. (2006). Mid-Holocene El Niño–Southern Oscillation (ENSO) attenuation revealed by individual foraminifera in eastern tropical Pacific sediments. *Geology*, *34*(12), 993–996. <https://doi.org/10.1130/G22810A.1>
- Leduc, G., Vidal, L., Cartapanis, O., & Bard, E. (2009). Modes of eastern equatorial Pacific thermocline variability: Implications for ENSO dynamics over the last glacial period. *Paleoceanography*, *24*(3). <https://doi.org/10.1029/2008PA001701>
- Liu, Z., Lu, Z., Wen, X., Otto-Bliesner, B. L., Timmermann, A., & Cobb, K. M. (2014). Evolution and forcing mechanisms of El Niño over the past 21,000 years. *Nature*, *515*(7528), 550–553.
<https://doi.org/10.1038/nature13963>
- Lombard, F., Labeyrie, L., Michel, E., Bopp, L., Cortijo, E., Retailleau, S., et al. (2011). Modelling planktic foraminifer growth and distribution using an ecophysiological multi-species approach. *Biogeosciences*, *8*(4), 853–873. <https://doi.org/10.5194/bg-8-853-2011>
- Lougheed, B. C. (2020). SEAMUS (v1.20): a $\Delta 14\text{C}$ -enabled, single-specimen sediment accumulation simulator. *Geoscientific Model Development*. <https://doi.org/10.5194/gmd-2019-155>
- Lyon, B., & Barnston, A. G. (2005). ENSO and the Spatial Extent of Interannual Precipitation Extremes in Tropical Land Areas. *Journal of Climate*, *18*(23), 5095–5109.
<https://doi.org/10.1175/JCLI3598.1>
- Metcalfe, B., Lougheed, B. C., Waelbroeck, C., & Roche, D. M. (2020). A proxy modelling approach to assess the potential of extracting ENSO signal from tropical Pacific planktonic foraminifera. *Climate of the Past*, *16*, 885–910. <https://doi.org/10.5194/cp-16-885-2020>
- Oba, T., & Uomonoto, K. (1989). Oxygen and Carbon Isotopic Ratios of Planktonic Foraminifera in Sediment Traps JT-01 and JT-02. *Gekkan Kaiyō*, *21*(4), 239–246.

- Peng, T.-H., Broecker, W. S., & Berger, W. H. (1979). Rates of benthic mixing in deep-sea sediment as determined by radioactive tracers. *Quaternary Research*, *11*(1), 141–149.
- Pisias, N. G. (1983). Geologic time series from deep-sea sediments: Time scales and distortion by bioturbation. *Marine Geology*, *51*(1–2), 99–113.
- Pracht, H., Metcalfe, B., & Peeters, F. J. C. (2019). Oxygen isotope composition of the final chamber of planktic foraminifera provides evidence of vertical migration and depth-integrated growth. *Biogeosciences*, *16*(2), 643–661. <https://doi.org/10.5194/bg-16-643-2019>
- Roche, D. M., Waelbroeck, C., Metcalfe, B., & Caley, T. (2018). FAME (v1.0): a simple module to simulate the effect of planktonic foraminifer species-specific habitat on their oxygen isotopic content. *Geoscientific Model Development*, *11*(9), 3587–3603. <https://doi.org/10.5194/gmd-11-3587-2018>
- Rongstad, B. L., Marchitto, T. M., Marks, G. S., Koutavas, A., Mekik, F., & Ravelo, A. C. (2020). Investigating ENSO-Related Temperature Variability in Equatorial Pacific Core-Tops Using Mg/Ca in Individual Planktic Foraminifera. *Paleoceanography and Paleoclimatology*, *35*(2), e2019PA003774. <https://doi.org/10.1029/2019PA003774>
- Rosenthal, Y., & Broccoli, A. J. (2004). In Search of Paleo-ENSO. *Science*, *304*(5668), 219–221. <https://doi.org/10.1126/science.1095435>
- Rustic, G. T., Koutavas, A., Marchitto, T. M., & Linsley, B. K. (2015). Dynamical excitation of the tropical Pacific Ocean and ENSO variability by Little Ice Age cooling. *Science*, *350*(6267), 1537–1541.
- Schiffelbein, P. (1984). Effect of benthic mixing on the information content of deep-sea stratigraphical signals. *Nature*, *311*(5987), 651. <https://doi.org/10.1038/311651a0>
- Scussolini, P., van Sebille, E., & Durgadoo, J. V. (2013). Paleo Agulhas rings enter the subtropical gyre during the penultimate deglaciation. *Climate of the Past*, *9*(6), 2631–2639. <https://doi.org/10.5194/cp-9-2631-2013>

- Spero, H. J., & Williams, D. F. (1990). Evidence for seasonal low-salinity surface waters in the Gulf of Mexico over the last 16,000 years. *Paleoceanography*, *5*(6), 963–975.
<https://doi.org/10.1029/PA005i006p00963>
- Thirumalai, K., Partin, J. W., Jackson, C. S., & Quinn, T. M. (2013). Statistical constraints on El Niño Southern Oscillation reconstructions using individual foraminifera: A sensitivity analysis. *Paleoceanography*, *28*(3), 401–412. <https://doi.org/10.1002/palo.20037>
- Thirumalai, K., DiNezio, P. N., Tierney, J. E., Puy, M., & Mohtadi, M. (2019). An El Niño Mode in the Glacial Indian Ocean? *Paleoceanography and Paleoclimatology*, *34*.
<https://doi.org/10.1029/2019PA003669>
- Trauth, M. H. (1998). TURBO: a dynamic-probabilistic simulation to study the effects of bioturbation on paleoceanographic time series. *Computers & Geosciences*, *24*(5), 433–441.
[https://doi.org/10.1016/S0098-3004\(98\)00019-3](https://doi.org/10.1016/S0098-3004(98)00019-3)
- Trauth, M. H. (2013). TURBO2: A MATLAB simulation to study the effects of bioturbation on paleoceanographic time series. *Computers & Geosciences*, *61*, 1–10.
<https://doi.org/10.1016/j.cageo.2013.05.003>
- Trauth, M. H., Sarnthein, M., & Arnold, M. (1997). Bioturbational mixing depth and carbon flux at the seafloor. *Paleoceanography*, *12*(3), 517–526.
- White, S. M., & Ravelo, A. C. (2020). Dampened El Niño in the Early Pliocene Warm Period. *Geophysical Research Letters*, *47*(4), e2019GL085504. <https://doi.org/10.1029/2019GL085504>
- White, S. M., Ravelo, A. C., & Polissar, P. J. (2018). Dampened El Niño in the Early and Mid-Holocene Due To Insolation-Forced Warming/Deepening of the Thermocline. *Geophysical Research Letters*, *45*(1), 316–326. <https://doi.org/10.1002/2017GL075433>

Table 1. Overview of SAR and number of picked specimens in select IFA studies (including non-ENSO studies). Region codes are as follows: WEP – Western Equatorial Pacific; CEP – Central Equatorial Pacific; EEP – Eastern Equatorial Pacific; EEI – Eastern Equatorial Indian Ocean; SIO – Southern Indian Ocean; ARA – Arabian Sea. We have estimated the 1σ value of age in 1 cm of sediment based on the SAR and a BD of 10 cm (Boudreau, 1998), using the following calculation based on (Berger & Heath, 1968): $BD/SAR \times 1000$, where SAR is entered in cm ka^{-1} and BD in cm.

Core(s)	Study	Region	Approximate SAR (cm ka^{-1})	Estimated 1σ value of age in 1 cm (yr)	Specimens picked per discrete interval (#)
MGL1208-14MC and 12GC	(White et al., 2018)	CEP	~2.5	4000	70 ~ 90
ODP 806	(Ford et al., 2015)	WEP	~ 3	3300	60 ~ 70
ODP 849	(Ford et al., 2015) (White & Ravelo, 2020)	EEP	~ 4	2500	60 ~ 70
KNR195-5 MC42	(Rustic et al., 2015)	EEP	~12	830	55
MD02-2529	(Leduc et al., 2009)	EEP	~40	250	65 ~ 90
V21-30	(Koutavas et al., 2006) (Koutavas & Joanides, 2012)	EEP	~12	830	50
MD98-2177	(Khider et al., 2011)	WEP	~70	150	60 ~ 90
SO189-119KL	(Thirumalai et al., 2019)	EEI	~20	500	55 ~ 65
SO189-39KL	(Thirumalai et al., 2019)	EEI	~ 37	270	55 ~ 65
GeoB 10038-4	(Thirumalai et al., 2019)	EEI	~9	1100	55 ~ 65
GeoB 10053-7	(Thirumalai et al., 2019)	EEI	~35	290	55 ~ 65

NIOP 905P	(Ganssen et al., 2011)	ARA	~20	500	30 ~ 40
64PE-174P13	(Scussolini et al., 2013)	SIO	~ 1.2	8330	20 ~ 30

Main figure captions

395 **Figure 1.** Overview of the modelled core site location and associated TRACE-21ka data. Panel a: The location of the modelled sediment core site superimposed upon the standard deviation of annualised SST from the TRACE-21ka for the 500 year period between 1490 CE and 1989 CE. Also shown for reference are the Niño regions 1+2, 3, 3.4 and 4. Panel b: 100 year (1200 month) and 1000 year (12000 month) moving mean the monthly TRACE-21ka SST data for the modelled sediment core site. Also shown in light blue and light grey are the moving $\pm 1\sigma$ envelopes respectively associated with the moving 100 year (1200 month) and 1000 year (12000 month) windows. Panel c: 100 year (1200 month) and 1000 year (12000 month) moving 1σ of the 1.5-7 year filtered monthly SST data.

405 **Figure 2.** Panel a: The dynamic species abundance function applied to some of the simulations in this study. Panel b: An theoretical example of how the dynamic species abundance would bias recording of SST by individual foraminifera. In blue, a normally distributed theoretical SST profile. In green, the signal that would be recorded by a species affected by the dynamic species abundance function.

410 **Figure 3.** Simulated downcore, discrete 1 cm depth 1σ SST values of simulated single foraminifera from various 40 cm ka^{-1} SAR scenarios with 10 cm BD, each with 100 ensembles of SEAMUS runs. In each panel, each ensemble is shown using a coloured line. The solid black lines represent the 95% interval of the ensemble runs at each discrete 1 cm depth. Also shown for reference as a thick grey line is the 1000 year (12000 month) moving 1σ of the 1.5-7 year filtered monthly SST data (as also shown in Fig. 1c.) The left panels (a, c, e and g) show the output of scenarios with 50, 100, 500 and 10^4 randomly picked foraminifera per discrete 1 cm depth, all with constant species abundance and no assumed analytical error. The right panels (b, d, f and h) show the output of scenarios with 50, 100, 500 and 10^4 randomly picked foraminifera per discrete 1 cm depth, all with constant species abundance and an assumed analytical error of $\pm 1^\circ\text{C}$ in SST.

420 **Figure 4.** Simulated downcore, discrete 1 cm depth 1σ SST values of simulated single foraminifera from various 40 cm ka^{-1} SAR scenarios with 10 cm BD, each with 100 ensembles of SEAMUS runs. In each panel, each ensemble is shown using a coloured line. The solid black lines represent the 95% interval of the ensemble runs at each discrete 1 cm depth. Also shown for reference as a thick grey line is the 1000 year (12000 month) moving 1σ of the 1.5-7 year filtered monthly SST data (as also shown in Fig. 1c. The left panels (a, c, e and g) show the output of scenarios with 50, 100, 500 and 10^4 randomly picked foraminifera per discrete 1 cm depth, all with dynamic species abundance (following Fig. 2a) and no assumed analytical error. The right panels (b, d, f and h) show the output of scenarios with 50, 100, 500

and 10^4 randomly picked foraminifera per discrete 1 cm depth, all with dynamic species abundance (following Fig. 2a) and an assumed analytical error of $\pm 1^\circ\text{C}$ in SST.

Figure 5. Simulated single foraminifera SST distributions from 100 ensembles of SEAMUS runs, with SAR of 40 cm ka^{-1} , BD of 10 cm, no analytical error and constant abundance. In each ensemble, the single foraminifera SST distribution from a single discrete depth with a simulated median age of 17.5 ka is shown, and compared to the TRACE-21ka SST distribution for the 18 ka to 17 ka period. The left panels (a, d, g and j) show the 100 SEAMUS ensembles as coloured lines in the case of 50, 100, 500 and 10^4 randomly picked foraminifera, with the TRACE-21ka SST distribution is shown as a black line. The middle panels (b, e, h and k) show the the rate of over/undersampling for each of the 100 SEAMUS ensembles (coloured lines) relative to the TRACE-21ka SST distribution (black line) in the case of 50, 100, 500 and 10^4 randomly picked foraminifera. The right panels (c, f, i and l) show Q-Q plots of the 100 SEAMUS ensemble quantiles vs the TRACE-21ka quantiles as coloured lines in the case of 50, 100, 500 and 10^4 randomly picked foraminifera, with a perfect 1:1 correspondence to TRACE-21ka shown for reference as a black line.

Figure 6. Simulated single foraminifera SST distributions from 100 ensembles of SEAMUS runs, with SAR of 40 cm ka^{-1} , BD of 10 cm, $\pm 1 \text{ }^\circ\text{C}$ analytical error and constant abundance. In each ensemble, the single foraminifera SST distribution from a single discrete depth with a simulated median age of 17.5 ka is shown, and compared to the TRACE-21ka SST distribution for the 18 ka to 17 ka period. The left panels (a, d, g and j) show the 100 SEAMUS ensembles as coloured lines in the case of 50, 100, 500 and 10^4 randomly picked foraminifera, with the TRACE-21ka SST distribution is shown as a black line. The middle panels (b, e, h and k) show the the rate of over/undersampling for each of the 100 SEAMUS ensembles (coloured lines) relative to the TRACE-21ka SST distribution (black line) in the case of 50, 100, 500 and 10^4 randomly picked foraminifera. The right panels (c, f, i and l) show Q-Q plots of the 100 SEAMUS ensemble quantiles vs the TRACE-21ka quantiles as coloured lines in the case of 50, 100, 500 and 10^4 randomly picked foraminifera, with a perfect 1:1 correspondence to TRACE-21ka shown for reference as a black line.

Figure 7. Simulated single foraminifera SST distributions from 100 ensembles of SEAMUS runs, with SAR of 40 cm ka^{-1} , BD of 10 cm, no analytical error and dynamic abundance (following Fig. 2a). In each ensemble, the single foraminifera SST distribution from a single discrete depth with a simulated median age of 17.5 ka is shown, and compared to the TRACE-21ka SST distribution for the 18 ka to 17 ka period. The left panels (a, d, g and j) show the 100 SEAMUS ensembles as coloured lines in the case of 50, 100, 500 and 10^4 randomly picked foraminifera, with the TRACE-21ka SST distribution is shown as a black line. The middle panels (b, e, h and k) show the the rate of over/undersampling for each of the 100 SEAMUS ensembles (coloured lines) relative to the TRACE-21ka SST distribution (black line) in the case of 50, 100, 500 and 10^4 randomly picked foraminifera. The right panels (c, f, i and l) show Q-Q

460 plots of the 100 SEAMUS ensemble quantiles vs the TRACE-21ka quantiles as coloured lines in the case of 50, 100, 500 and 10^4 randomly picked foraminifera, with a perfect 1:1 correspondence to TRACE-21ka shown for reference as a black line.

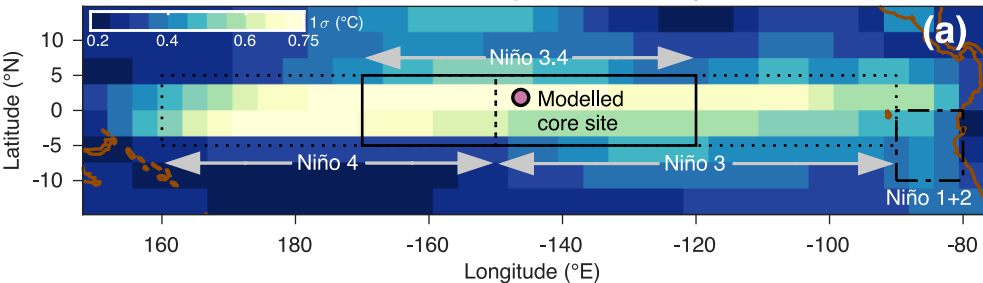
Figure 8. Simulated single foraminifera SST distributions from 100 ensembles of SEAMUS runs, with SAR of 40 cm ka^{-1} , BD of 10 cm, $\pm 1 \text{ }^\circ\text{C}$ analytical error and dynamic abundance (following Fig. 2a). In each ensemble, the single foraminifera SST distribution from a single discrete depth with a simulated median age of 17.5 ka is shown, and compared to the TRACE-21ka SST distribution for the 18 ka to 17 ka period. The left panels (a, d, g and j) show the 100 SEAMUS ensembles as coloured lines in the case of 50, 100, 500 and 10^4 randomly picked foraminifera, with the TRACE-21ka SST distribution is shown as a black line. The middle panels (b, e, h and k) show the the rate of over/undersampling for each of the 100 SEAMUS ensembles (coloured lines) relative to the TRACE-21ka SST distribution (black line) in the case of 50, 100, 500 and 10^4 randomly picked foraminifera. The right panels (c, f, i and l) show Q-Q plots of the 100 SEAMUS ensemble quantiles vs the TRACE-21ka quantiles as coloured lines in the case of 50, 100, 500 and 10^4 randomly picked foraminifera, with a perfect 1:1 correspondence to TRACE-21ka shown for reference as a black line.

465

470

Figure 1.

TRACE-21ka annualised surface temperature variability (1490 CE to 1989 CE)



TRACE-21ka monthly time series for modelled core site

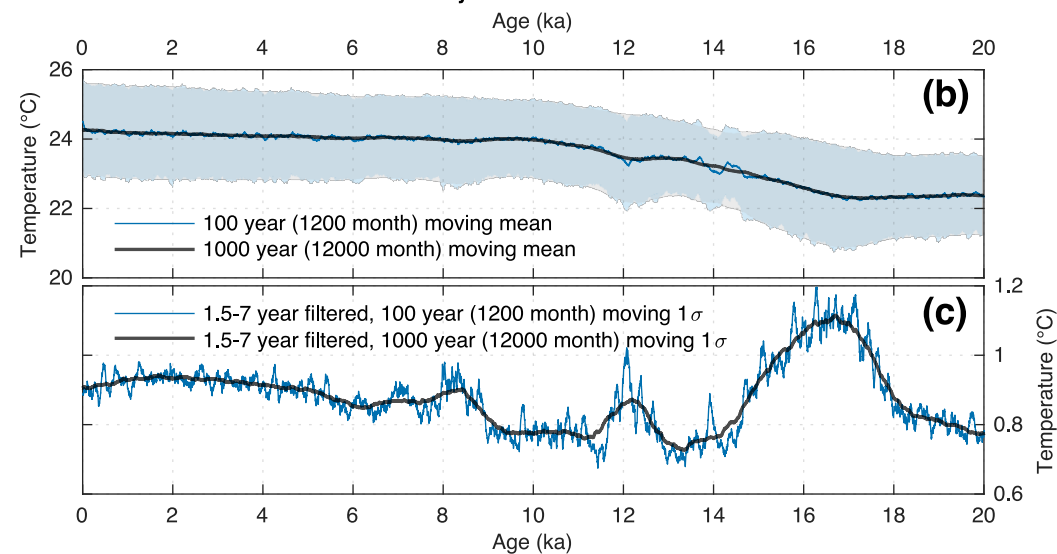
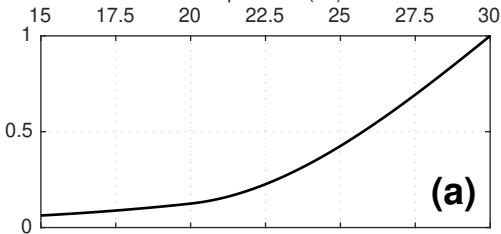



Figure 2.


Dynamic species abundance

Temperature (°C)

Relative abundance



 Theoretical original profile ($\mu=23$, skew=0)

 Abundance-modified profile ($\mu=23.9$, skew=-0.08)

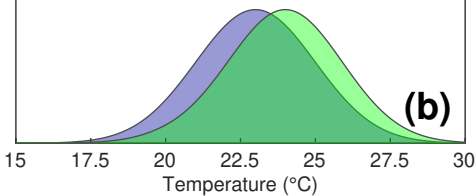
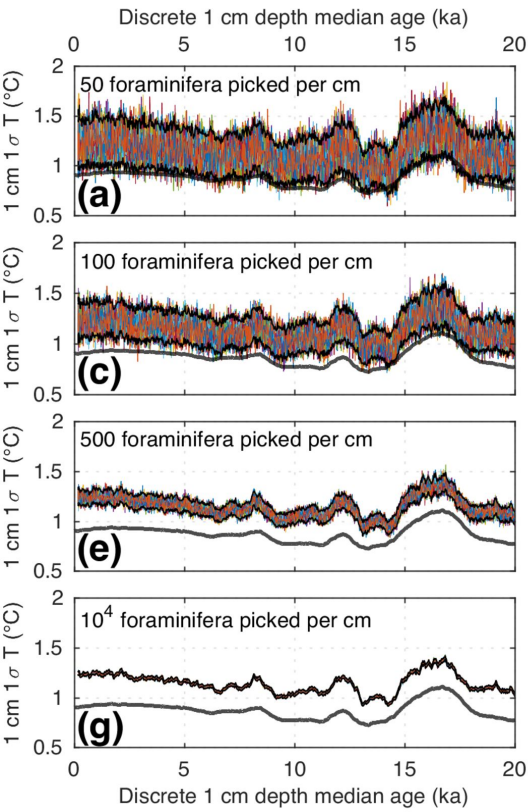


Figure 3.

Ensemble of 100 SEAMUS core simulations
SAR: 40 cm ka⁻¹, BD: 10 cm, no error
and constant abundance



Ensemble of 100 SEAMUS core simulations
SAR: 40 cm ka⁻¹, BD: 10 cm, $\pm 1^\circ\text{C}$ error
and constant abundance

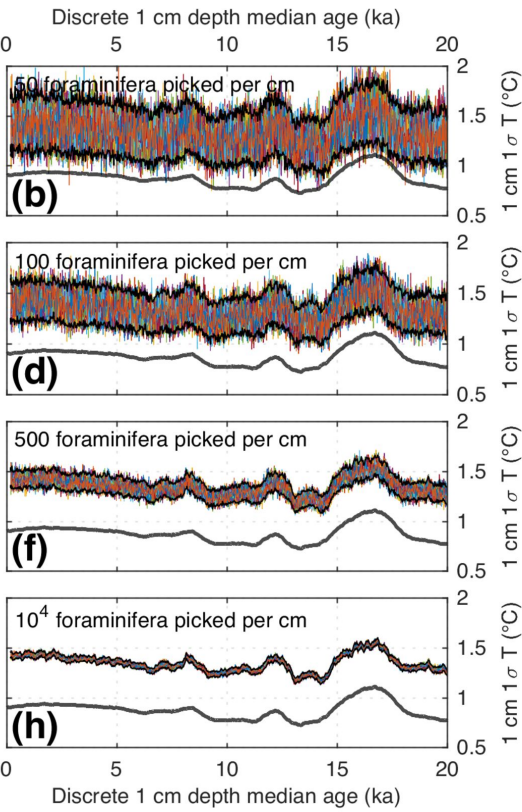


Figure 4.

Ensemble of 100 SEAMUS core simulations
SAR: 40 cm ka⁻¹, BD: 10 cm, no error
and dynamic abundance

Ensemble of 100 SEAMUS core simulations
SAR: 40 cm ka⁻¹, BD: 10 cm, ±1°C error
and dynamic abundance

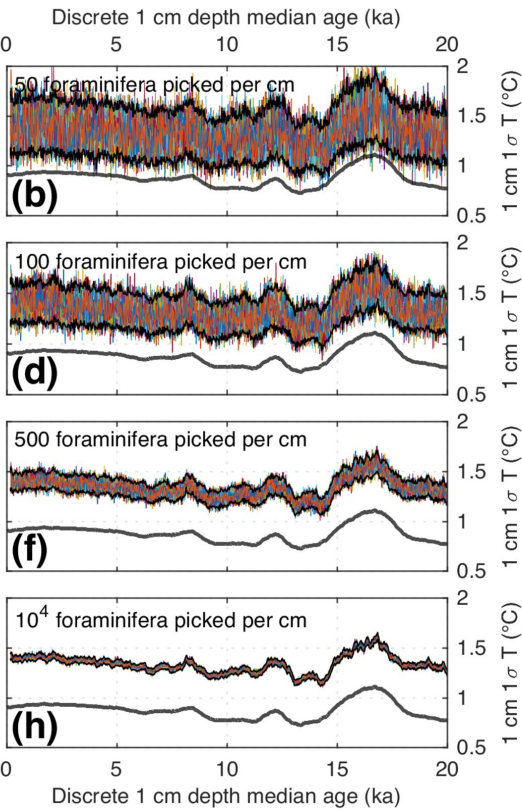
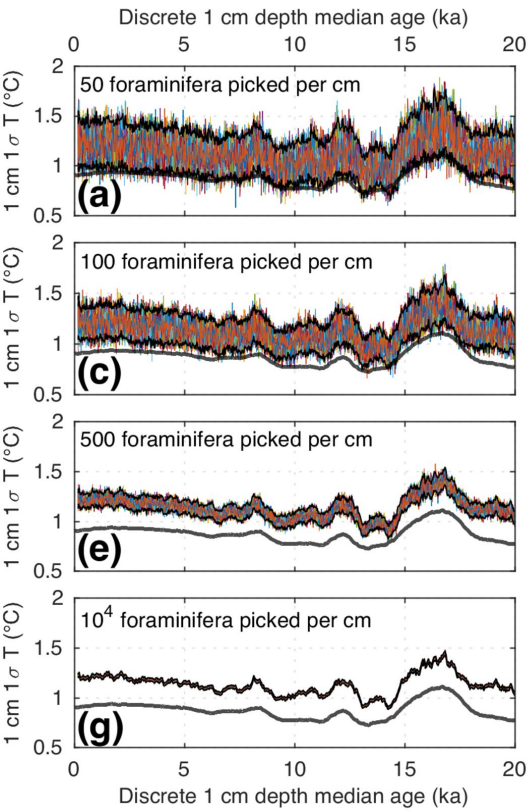


Figure 5.

Ensemble of 100 SEAMUS runs compared to TRACE21ka for period spanning 18 ka to 17 ka.
SAR: 40 cm ka⁻¹, BD: 10 cm, no analysis error and constant abundance

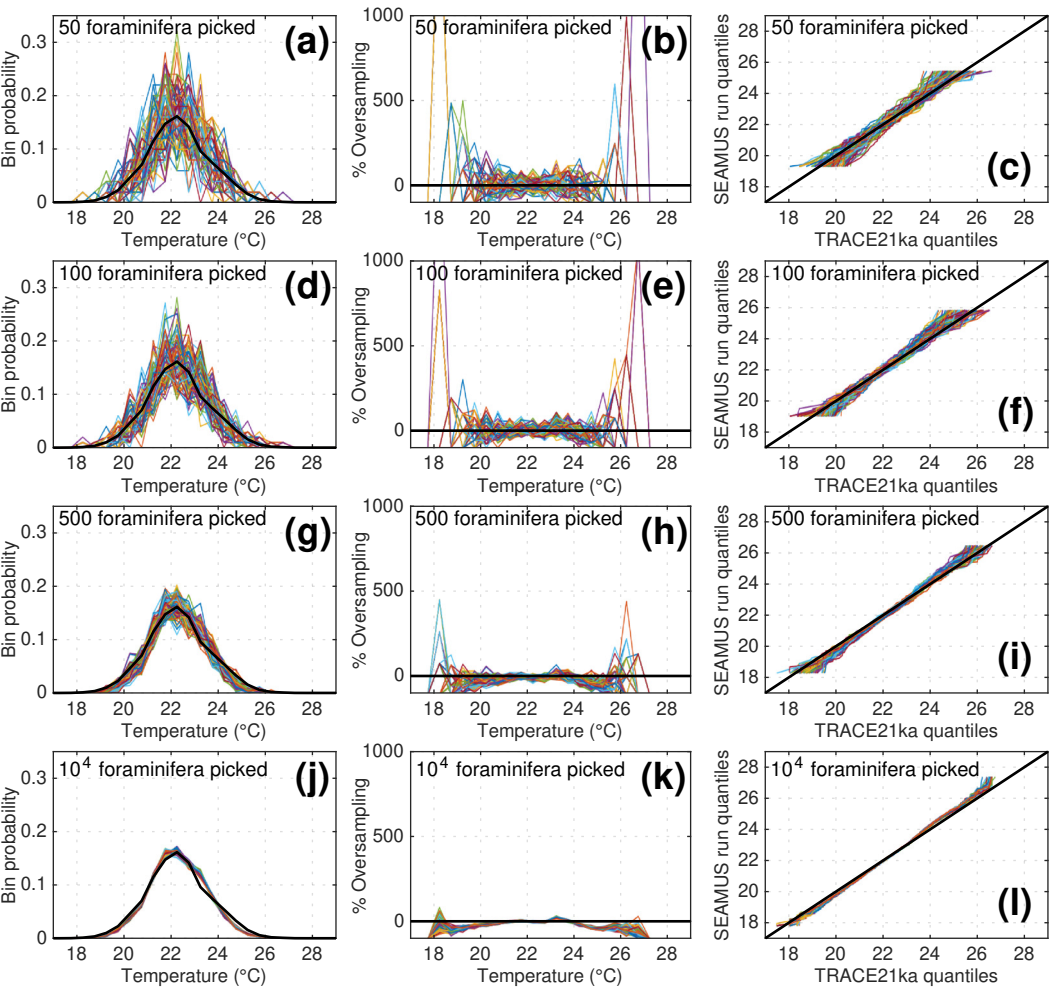


Figure 6.

Ensemble of 100 SEAMUS runs compared to TRACE21ka for period spanning 18 ka to 17 ka.
SAR: 40 cm ka⁻¹, BD: 10 cm, ±1°C analysis error and constant abundance

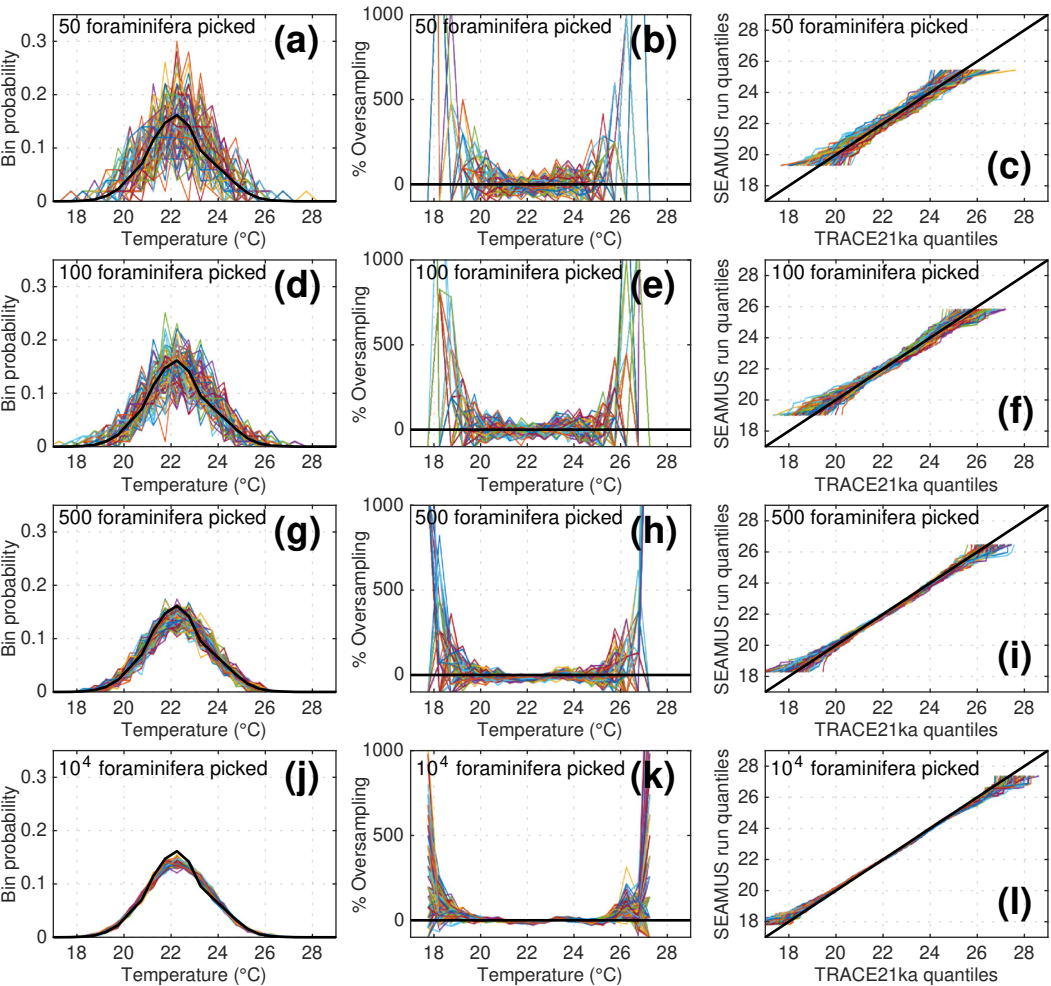


Figure 7.

Ensemble of 100 SEAMUS runs compared to TRACE21ka for period spanning 18 ka to 17 ka.
SAR: 40 cm ka⁻¹, BD: 10 cm, no analysis error and dynamic abundance

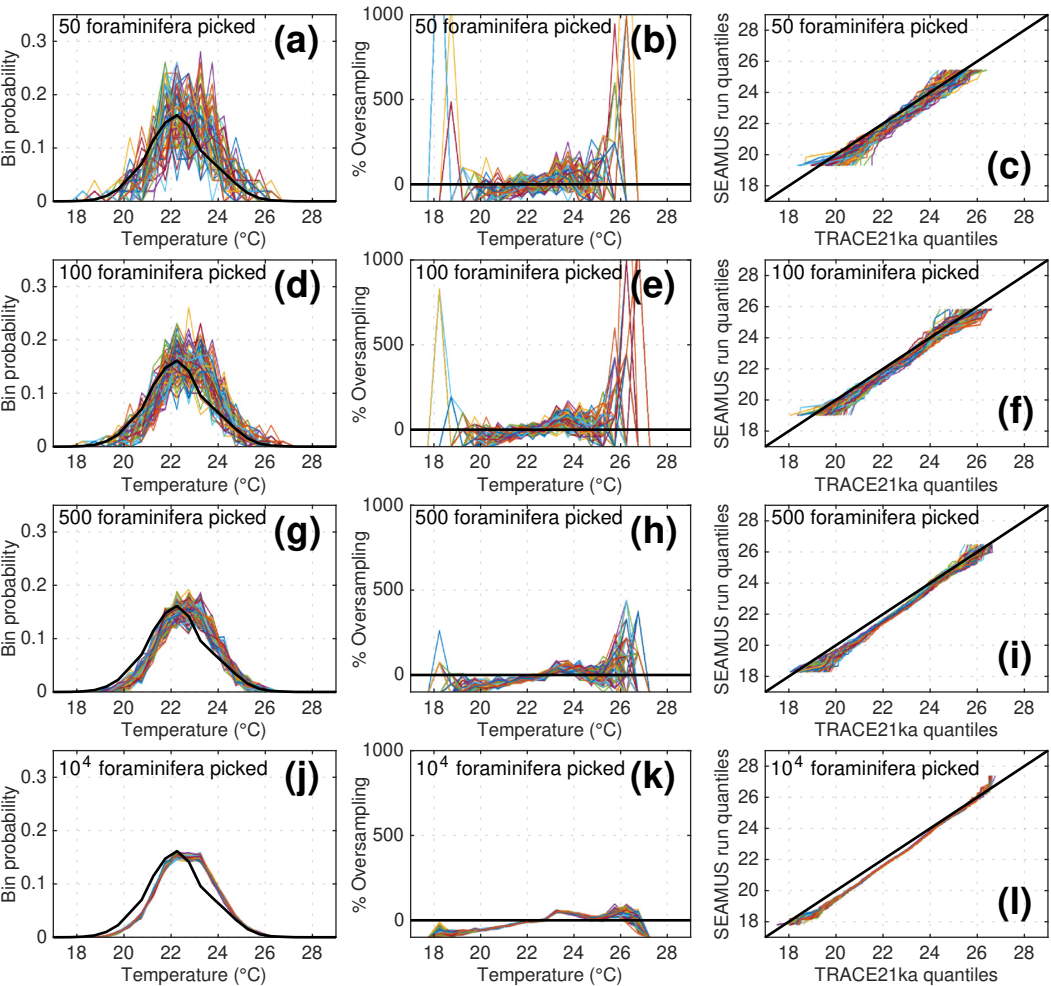


Figure 8.

Ensemble of 100 SEAMUS runs compared to TRACE21ka for period spanning 18 ka to 17 ka.
SAR: 40 cm ka⁻¹, BD: 10 cm, ±1°C analysis error and dynamic abundance

